Journal of Organometallic Chemistry, 383 (1990) 253–269
Elsevier Sequoia S.A., Lausanne – Printed in The Netherlands
JOM 20158

The syntheses, structures, and stereodynamics of [3]-ferrocenophane complexes

III. Rhenium tricarbonyl halide complexes, *fac*-$[ReX(CO)_3\{(C_5H_4ECH_3)_2Fe\}]$ (X = Cl, Br, I; E = S, Se). Crystal structure of chloro-1,1′-bis(methylthio)ferrocenetricarbonylrhenium

Edward W. Abel, Nicholas J. Long, Keith G. Orrell, Anthony G. Osborne, Vladimir Šik,

Department of Chemistry, The University, Exeter, Devon EX4 4QD (U.K.)

Paul A. Bates and Michael B. Hursthouse

Department of Chemistry, Queen Mary College, London E1 4NS (U.K.)

(Received April 24th, 1989)

Abstract

The complexes *fac*-$[ReX(CO)_3\{(C_5H_4ECH_3)_2Fe\}]$ (X = Cl, Br, I; E = S, Se) have been synthesised. A ^1H NMR study of their solution properties showed that pyramidal inversion of the coordinated chalcogen atoms was rapid on the NMR timescale at ambient temperatures, but at low temperatures (ca. −70 °C) the complexes existed as mixtures of *meso* and DL species, with the former predominating, particularly in the sulphur ligand complexes. Low temperature 2D-EXSY studies and variable temperature 1D bandshape analyses yielded accurate chalcogen inversion energies for both *meso*-1 → DL-1 and DL-1 → DL-1 exchanges. Values of $\Delta G^{\ddagger}$(298 K) for these interconversions were, respectively, in the regions of 43 and 46 kJ mol^{-1} (S inversion) and 63 and 66 kJ mol^{-1} (Se inversion). The crystal structure of chloro-1,1′-bis(methylthio)ferrocenetricarbonylrhenium has been determined. The crystals have space group $P\bar{1}$, with a 9.030(1), b 14.252(2), c 7.554(1) Å, α 76.58(1)°, β 104.73(1)°, γ 107.08(1)° and $Z = 2$. Least-squares refinement gave $R = 0.030$ for 2930 reflections. The Re–S bond lengths are 2.504(4) and 2.512(4) Å and the S–Me groups adopt a *meso* relationship analogous to the preferred solution structure. The S–Re–S bond angle is 80.0(2)° and the non-bonded S–S separation

0022-328X/90/$03.50

3.224 Å. The cyclopentadienyl rings adopt an eclipsed conformation with the ring planes parallel.

Introduction

In recent years we have carried out a wide-ranging study of the intramolecular motions exhibited by some transition metal complexes that contain at least one chalcogen atom bonded to the transition metal. These studies, which involved detailed dynamic NMR measurements, have enabled us to identify a number of unusual intramolecular rearrangements and to measure the associated energy barriers [1].

As a continuation of this work we have commenced a study of the metal complexes formed by certain organometallic chalcogen containing ligands in which a metallocene fragment forms the backbone of the ligand, e.g. 1,1′-bis(methylthio)ferrocene, (BMSF), and 1,1′-bis(methylseleno)ferrocene, (BMSEF). In this context we have recently reported our studies on the complexes formed by these two ligands with the Group VI carbonyls [2], and with the organoplatinum halides, $[(PtXMe_3)_4]$ (X = Cl, Br, I) [3].

We now report the synthesis and spectroscopic properties of the complexes *fac*-$[ReX(CO)_3(L–L)]$, (X = Cl, Br, I; L–L = BMSF, BMSEF), their chalcogen inversion energies, and the crystal and molecular structure of $[ReCl(CO)_3(BMSF)]$.

Experimental

General

All preparations were carried out using standard Schlenk techniques [4]. All solvents were freshly distilled, dried and degassed before use and all reactions were performed under purified nitrogen.

The following materials were prepared according to literature methods; $ReX(CO)_5$ (X = Cl, Br, I) [5,6], 1,1′-bis(methylthio)ferrocene (BMSF) and 1,1′-bis(methylseleno)ferrocene (BMSEF) [2].

Infrared spectra were recorded on a Perkin–Elmer 881 infrared spectrophotometer, calibrated from the 1602 cm^{-1} signal of polystyrene.

Elemental analyses were carried out by Butterworth Laboratories Ltd., Teddington, Middlesex, London and by C.H.N. Analysis, South Wigston, Leicester.

Synthesis of complexes

All the complexes were prepared in a similar way, the only difference being the time of reaction. Details of the synthetic, analytical and infrared data are given in Table 1 and a representative example of a preparation is outlined below.

$ReBr(CO)_5$ (0.25 g, 0.62 mmol) was dissolved in tetrahydrofuran (40 cm^3), BMSF (0.20 g, 0.72 mmol) was added, and the mixture was stirred and refluxed for 10 h. The progress of the reaction was monitored by infrared spectroscopy. The orange solution was filtered and evaporated to dryness. The resulting solid was washed with hexane and recrystallised from dichloromethane/hexane (1/1) to produce orange crystals of $[ReBr(CO)_3(BMSF)]$. Yield 0.259 g (66%).

NMR Studies

^1H and ^{13}C-{^1H} NMR spectra were recorded on a Bruker AM250 Spectrometer, operating at 250.13 and 62.90 MHz respectively. A ^1H spectrum of complex **2** was recorded on a Bruker WH400 Spectrometer at the University of Warwick.

All spectra were recorded in CD_2Cl_2 or $CDCl_3$ solutions with Me_4Si as the internal standard.

A standard B-VT1000 variable temperature unit was used to control the probe temperature, the calibration of this unit being checked periodically against a Comark digital thermometer. The temperatures are considered accurate to $\pm 1°C$.

^1H 2D-EXSY spectra for complexes **1**, **2**, **3** and **6** were recorded as previously reported [7,8] using the Bruker automation program NOESYPH. In the two-dimensional experiments, for complexes **1**, **2** and **3**, the F1 dimension contained 256 words which was then zero-filled to 1000 words, and the F2 dimension contained 1000 words. The spectral width was 800 Hz. The mixing time, τ_m, was 1 second, with a maximum random variation of 10%. The number of scans per experiment was 4, giving a total experimental time of 2 h. The data were processed using a gaussian window function of size 1 Hz in both dimensions and symmetrised about the diagonal.

In the two-dimensional experiment for complex **6** the parameters were slightly different. The F1 dimension contained 64 words, then zero-filled to 256, and the F2 dimension contained 256 words. The spectral width was 262 Hz, and the mixing time, τ_m, was 1 second, again with a maximum random variation of 10%. The number of scans per experiment was 32, giving a total experimental time of 4 h. The data were processed using a gaussian window function of size 1 Hz in both dimensions and symmetrised about the diagonal.

Bandshape analyses were performed using modified versions of the program DNMR of Kleier and Binsch [9,10].

X-ray structure determination

Crystal data for $C_{15}H_{14}ClFeO_3ReS_2$: $M = 583.89$, triclinic, space group $P\bar{1}$, a 9.030(1), b 14.252(2), c 7.554(1) Å, α 76.58(1)°, β 104.73(1)°, γ 107.08(1)°, U 885.6(2) Å^3, $Z = 2$, D_c 2.190 g cm^{-3}, $F(000) = 556$, λ 0.71069 Å, μ(Mo-K_α) 81.30 cm^{-1}, crystal size 0.63 × 0.38 × 0.23 mm.

Data collection. Unit cell parameters and intensity data were obtained by following previously detailed procedures [11], using a CAD4 diffractometer operating in the ω-2θ scan mode, with graphite-monochromated Mo-K_α radiation.

A total of 3094 unique reflections were collected ($3 \leqslant 2\theta \leqslant 50°$). The segment of reciprocal space scanned was: h, −10–10; k, −16–16; l, 0–9. The reflection intensities were corrected for absorption using the azimuthal-scan method [12]; maximum and minimum transmission factors 1.00, 0.38.

Solution and refinement of structure. The structure was solved by the application of routine heavy-atom methods (SHELX-84) [13], and refined by full-matrix least-squares (SHELX-76) [14]. All non-hydrogen atoms were refined anisotropically and hydrogen atoms were not included in the final model.

The final residuals R and R_w were 0.030 and 0.034 respectively for the 208 variables and 2930 reflections for which $F_o > 6\sigma(F_o)$. The function minimised was $\Sigma w(|F_o| - |F_c|)^2$, with the weight, w, being defined as $1/[\sigma^2(F_o) + gF_o^2]$ (g = 0.003).

Table 1

Syntheses and characterisation of the complexes *fac*-[ReX(CO)$_3$(L–L)] (X = Cl,Br,I; (L–L) = chelating ferrocenylchalcogenide)

Complex	Reaction Time (h)	Yield [a] (%)	Melting Point (°C)	ν(CO) [b] (cm^{-1})			Analytical Data (Found (calcd.) (%))	
							C	H
fac-[ReCl(CO)$_3$(BMSF)] **(1)**	10	70	204–206	2032(s)	1939(vs)	1903(s)	30.9 (30.9)	2.4 (2.4)
fac-[ReBr(CO)$_3$(BMSF)] **(2)**	10	66	226–228 (dec.)	2033(s)	1941(vs)	1902(s)	28.9 (28.7)	2.3 (2.2)
fac-[ReI(CO)$_3$(BMSF)] **(3)**	68	51	223–225 (dec.)	2031(s)	1944(vs)	1901(s)	26.8 (26.7)	2.1 (2.1)
fac-[ReCl(CO)$_3$(BMSEF)] **(4)**	16	49	150–152	2030(s)	1933(s)	1901(s)	26.3 (26.6)	2.0 (2.1)
fac-[ReBr(CO)$_3$(BMSEF)] **(5)**	16	53	181–183	2031(s)	1936(s)	1902(s)	25.1 (24.9)	2.0 (1.9)
fac-[ReI(CO)$_3$(BMSEF)] **(6)**	70	44	185–187	2030(s)	1938(s)	1903(s)	23.4 (23.4)	1.8 (1.8)

[a] Yields quoted relative to [ReX(CO)$_5$]. [b] Recorded in CH_2Cl_2 solution, (s) = strong, (vs) = very strong.

Atomic scattering factors and anomalous scattering parameters were taken from ref. 15 and 16 respectively *. All computations were made on a DEC VAX-11/750 computer.

Results and discussion

The ligands BMSF and BMSEF react smoothly with rhenium pentacarbonyl halides in boiling tetrahydrofuran to give good yields of the complexes *fac*-[ReX(CO)$_3$(BMSF)] and *fac*-[ReX(CO)$_3$(BMSEF)], (X = Cl, Br, I). With both ligands the iodo complex required a much longer reaction time than the chloro and bromo complexes. All the products are air-stable, orange, crystalline materials, which are soluble in organic solvents. In the carbonyl stretching region of their infrared spectra the compounds show the pattern of three peaks expected for the *fac*-configuration, Table 1.

Static NMR spectra

Low temperature ^{1}H spectra of the complexes in CD_2Cl_2 or $CDCl_3$ solvents were recorded at -70 or $-80\,^\circ$C for the S-ligand (BMSF) complexes and at $-20\,^\circ$C for the Se-ligand (BMSEF) complexes. Two solution species were clearly identified from the numbers of signals present in the E-methyl (E = S, Se) and ring methine regions of the spectra (Tables 2, 3). In the BMSEF series of complexes (Table 3), a DL species was identified by its equal-intensity pair of Se-methyl signals, the other solution species being a *meso* form in which the Se-methyls were equivalent. The relative populations of these species were very halogen dependent, with the *meso* structure being increasingly favoured with increasing halogen mass/size (Table 3). For the BMSF complexes characterisation of the solution species was made from the methine proton signals since the pairs of S-methyl signals expected for the DL species could not always be identified because of overlap with the *meso* signal (Table 2). However, the methine regions of the spectra of all three BMSF complexes exhibited four strong signals of equal intensity and up to eight equal intensity weaker signals. The former set is clearly due to a *meso* structure which possesses a mirror plane containing the Pt and Fe atoms, thus rendering corresponding methine protons of each ring chemically equivalent. In the BMSF series, a *meso* form therefore is the predominant solution species, particularly in the X = Br and I complexes where the DL form is only just detectable.

Full ^{1}H NMR data for all six complexes are given in Tables 2 and 3. The ring methine protons exhibited weak vicinal H–H couplings which were not analysed. In the BMSEF series, the Se-methyl signals showed ^2J(SeH) couplings of magnitude 9.3–10.0 Hz (Table 3).

Low and ambient temperature ^{13}C spectra were recorded for the complex [ReBr(CO)$_3$(BMSF)]. The data are given in Table 4 where it should be noted that the *meso* and DL solution species can be clearly differentiated by their S-methyl and ring methine carbon shifts.

* A table of observed and calculated structure amplitudes and a complete list of anisotropic thermal parameters have been deposited with the British Library at Boston Spa, Wetherby, LS23 7BQ (U.K.) as Supplementary Publication.

Table 2

Hydrogen-1 NMR parameters for the complexes **1**–**3** in CD_2Cl_2 at ambient and low temperatures

Complex	Temperature (°C)	Solution species	Invertomer population (%)	Chemical shift S-Me protons (δ)	Chemical shift ring protons (δ) [a]	
1	−70	*meso*	66	2.84	4.91	4.71
					4.49	4.26
		DL	34	2.84	5.16 [b]	4.61
				2.77	4.56	4.52
					4.38	
	30	*meso*/DL	100	2.89	4.92	4.73
					4.43	4.37
2	−95 [c]	*meso*	81	2.86	4.90	4.72
					4.49	4.27
		DL	19	2.88	5.17 [b]	4.62
				2.85	4.58	4.53
					4.37	
	20	*meso*/DL	100	2.89	4.88	4.78
					4.47	4.36
3	−80	*meso*	90	2.82	4.87	4.72
					4.49	4.26
		DL	10	2.90	5.04 [b]	4.83
				2.82		
	30	*meso*/DL	100	2.92	4.86(2)	4.50
					4.35	

[a] Signals show weak multiplet structure in most cases. [b] Some DL signals not observed due to overlap. [c] Data measured at 400 MHz.

Dynamic NMR Spectra

All the above spectral details refer to apparently 'static' solution species since on raising the solution temperatures towards ambient values, gross changes occurred in the methine and E-methyl regions of the spectra. In the E-methyl region, the two S-Me signals or three Se-Me signals underwent exchange and coalesced to single averaged signals. In the methine region more complex changes took place with the limiting fast-exchange spectra consisting of four equal-intensity signals. Two possible intramolecular rate processes may be the cause of these observed spectral changes, namely pyramidal inversion of the coordinated chalcogen atoms and conformational changes of the bridge section of the ferrocenophane ring, as described in earlier parts of this work [2,3]. If both processes are slow on the NMR timescale, six distinguishable species can exist, namely four *meso* species and two enantiomeric DL pairs (Fig. 1). These structures may be interconverted either by inversion of a chalcogen atom (E^1 or E^2) or by reversal of the E–Re–E bridge linking the two ferrocenyl rings, changing the pseudo-ring from one half-chair form to another, (BR). However, this bridge reversal process may be safely assumed to be rapid on the NMR timescale at all observed temperatures for the same reasons as given for the $PtXMe_3$-ferrocenophane complexes [3], with which the present $ReX(CO)_3$ complexes are isoelectronic. Rapid bridge reversal implies that the solution structures are weighted averages of the adjacent structures on the front and rear faces of the cube diagram (Fig. 1). The spectral changes will then be a result of

Table 3

Hydrogen-1 NMR parameters for the complexes **4–6** in $CDCl_3$ at high and low temperatures

Complex	Temperature (°C)	Solution species	Invertomer population (%)	Chemical Shift Se-Me protons (δ)		Chemical shift ring protons (δ) [a]	
4	−20	*meso*	38	2.77	[9.5] [b]	4.87	4.59
						4.51	4.29
		DL	62	2.72	[9.3] [b]	5.15 [d]	4.56
				2.70	[9.8] [b]	4.41	4.33
						4.29	
	75	*meso*/DL	100	2.74	[9.9] [b]	4.86	4.60
						4.39	4.35
5	−20	*meso*	52	2.74 [c]		4.87	4.56
						4.51	4.29
		DL	48	2.76	[9.4] [b]	5.18 [d]	4.56
				2.71	[9.6] [b]	4.41	4.33
						4.30	
	70	*meso*/DL	100	2.75	[10.0] [b]	4.83	4.64
						4.41	4.35
6	−20	*meso*	65	2.74	[9.6] [b]	4.86	4.58
						4.53	4.28
		DL	35	2.82	[9.8] [b]	5.14	4.55
						4.51	4.50
				2.70	[9.7] [b]	4.49	4.41
						4.33	4.32
	70	*meso*/DL	100	2.77	[9.9] [b]	4.78	4.70
						4.43	4.33

[a] Signals show weak multiplet structure in most cases. [b] ^2J(SeH) (Hz) values. [c] ^{77}Se satellites obscured due to overlapping signals. [d] Some DL signals obscured due to overlap.

chalcogen inversion between the bridge-reversal-averaged DL pairs and one of the similarly averaged *meso* species.

The four structures comprising the rear face of the cube diagram involve a halogen atom X in close proximity to the ferrocenyl moiety and are therefore unfavoured on energy grounds. The partial structures comprising the front face of the cube (Fig. 1) are therefore close representations of the actual solution structures

Table 4

Carbon-13 NMR shifts for complex **2** in CD_2Cl_2 solution at ambient and low temperatures

Complex	Temperature (°C)	Invertomer	Chemical shift S-Me carbons (δ)	Chemical shift methine carbons (δ)			
2	−70	*meso*	30.2	77.0	75.3	73.2	70.8 [a]
		DL	33.3	76.9	75.7	74.3	74.1
			26.9	73.2	72.8	72.1	78.8 [b,c]
	30	*meso*/DL	29.6	75.7	75.0	72.8	71.8 [c]

[a] Additional signal at δ 81.7 (quaternary C?). [b] Assignment of this signal uncertain. [c] Quaternary C signal(s) undetected.

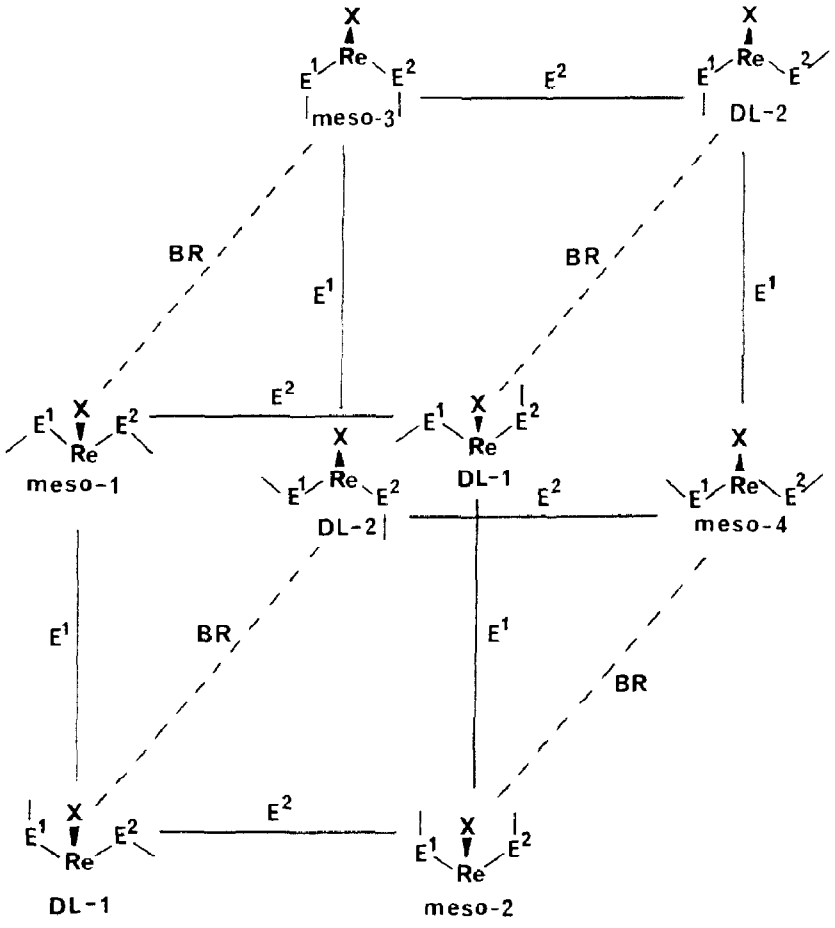

Fig. 1. Graph diagram showing the relationships of the static structures of $[ReX(CO)_3\{(C_5H_4ECH_3)_2Fe\}]$ (E = S, Se; X = Cl, Br, I) and their interconversion due to reversal of the E–Re–E portion of the ring (BR) and chalcogen inversion (E^1,E^2).

and the dynamic exchange process detected by the variable temperature NMR spectra essentially involves exchange between the two DL-1 forms and either the *meso*-1 or *meso*-2 form. Three pieces of evidence point to *meso*-1 being the NMR detectable solution species. Firstly, in the chelate complexes $[ReX(CO)_3\{MeE(CH_2)_2EMe\}]$ (E = S, Se; X = Cl, Br, I) [17] the *meso* invertomer with the E-methyls *trans* to X is more abundant in all cases except that of the complex E = S, X = Cl. (N.B. In that earlier work [17] the *meso*-1 and *meso*-2 labels were opposite to the present convention). Secondly, the populations of this *meso* form increased greatly with halogen mass/size in line with the present trends (Tables 2, 3), whereas the other *meso* form showed the opposite trend. Thirdly, the X-ray crystal structure of $[ReCl(CO)_3(BMSF)]$ (see later) shows that the S-methyl groups adopt a *meso* relationship analogous to the *meso*-1 solution structure. The assignment of *meso*-1 as the predominant low temperature solution form of the present complexes (except for $[ReCl(CO)_3(BMSEF)]$ where the DL-1 pair predominates) is therefore made with confidence. The above arguments are summarised by the structures shown in Fig. 2, which also provides the labelling of the methine protons.

The methine signals in the ^1H spectra of all the complexes showed the greatest degrees of exchange broadening due to the pyramidal inversions of the chalcogens and therefore this region was chosen for quantitative analysis of the inversion rates. Neglecting all scalar couplings since these are of low magnitude (estimated < 2.5 Hz) and not always resolved, the total methine spin problem then consists of four non-interacting exchange problems, namely:

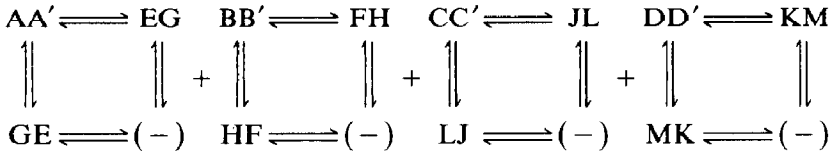

Since all scalar spin–spin couplings between the ferrocene rings can be neglected, the problem simplifies without loss of accuracy to four single spin exchanges between three different chemical configurations, two associated with the DL-1 structures and one with the *meso*-1 structure, namely:

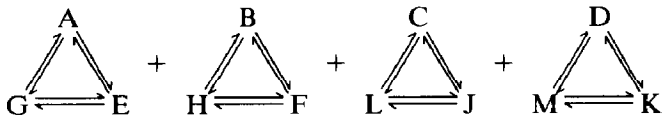

In order to undertake bandshape analysis of this problem it is necessary to identify the four sets of exchanging proton signals. This information can be neatly provided by 2D-EXSY NMR experiments just below the temperature at which exchange broadening is detected. The example of $[ReCl(CO)_3(BMSF)]$ is illustrated in Fig. 3. The 2D-EXSY spectrum at $-60\,^\circ C$ clearly reveals exchange between the four strong signals (labelled A–D) associated with the *meso*-1 species and the weaker signals (labelled E–K) due to the DL-1 pair. It should be stressed that the precise assignments of these methine signals to the chemical environments depicted in Fig. 2 cannot be known with great certainty. However, all that is required as a starting point for the band-shape analysis is the identification of the four sets of exchanging triplets of signals. Such information is provided unambiguously by the 2D-EXSY spectra and the labelling shown in Fig. 2 is fully consistent with this analysis. Whilst the assignments of the *meso*-1 methine signals are fairly certain, the labelling of the DL methine pairs, G/E, H/F, L/J and M/K might well be reversed, but such changes would produce no effect whatsoever on any subsequent bandshape analyses.

Bandshape fittings were carried out on all the complexes except $[ReI(CO)_3(BMSF)]$, where the very low abundance of the DL species caused very little exchange broadening in the variable temperature NMR spectra. Spectra of $[ReCl(CO)_3(BMSF)]$ in the temperature range -70 to $-10\,^\circ C$ are shown in Fig. 4, together with computer simulated spectra based on the dynamic spin system given above. These spectra were sensitive to two rate constants, namely k_1(*meso*-1 → DL-1) and k_2(DL-1 → DL-1) and the optimum values for each temperature are given in Fig. 4. It should be noted that the rate constants k_2(DL-1 → DL-1) refer to the net effect of both chalcogen atoms inverting. However, this double inversion process almost certainly proceeds via the undetected *meso*-2 structure, since rates of synchronous inversion of chalcogen pairs have been shown to be negligibly small compared to

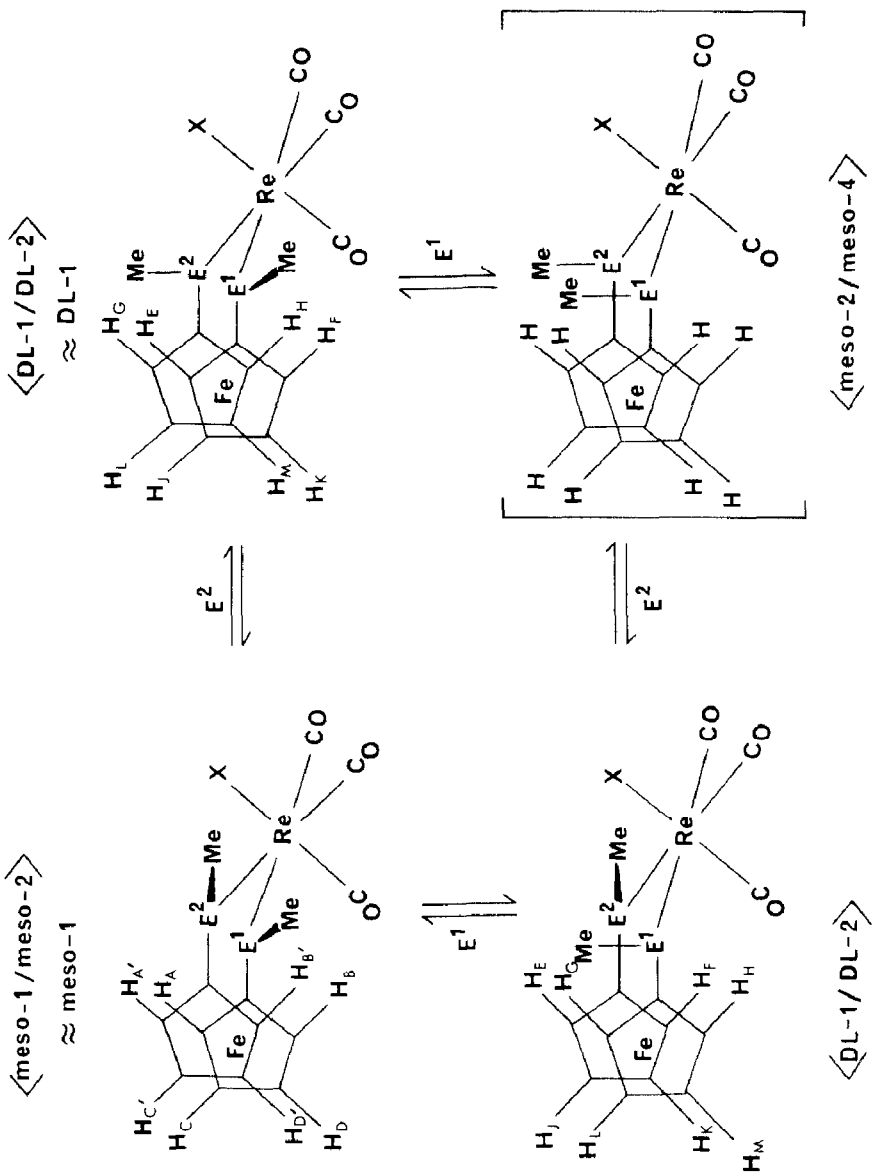

Fig. 2. The bridge-reversal-averaged invertomers of the complexes $[ReX(CO)_3\{(C_5H_4ECH_3)_2Fe\}]$ showing the methine proton labelling.

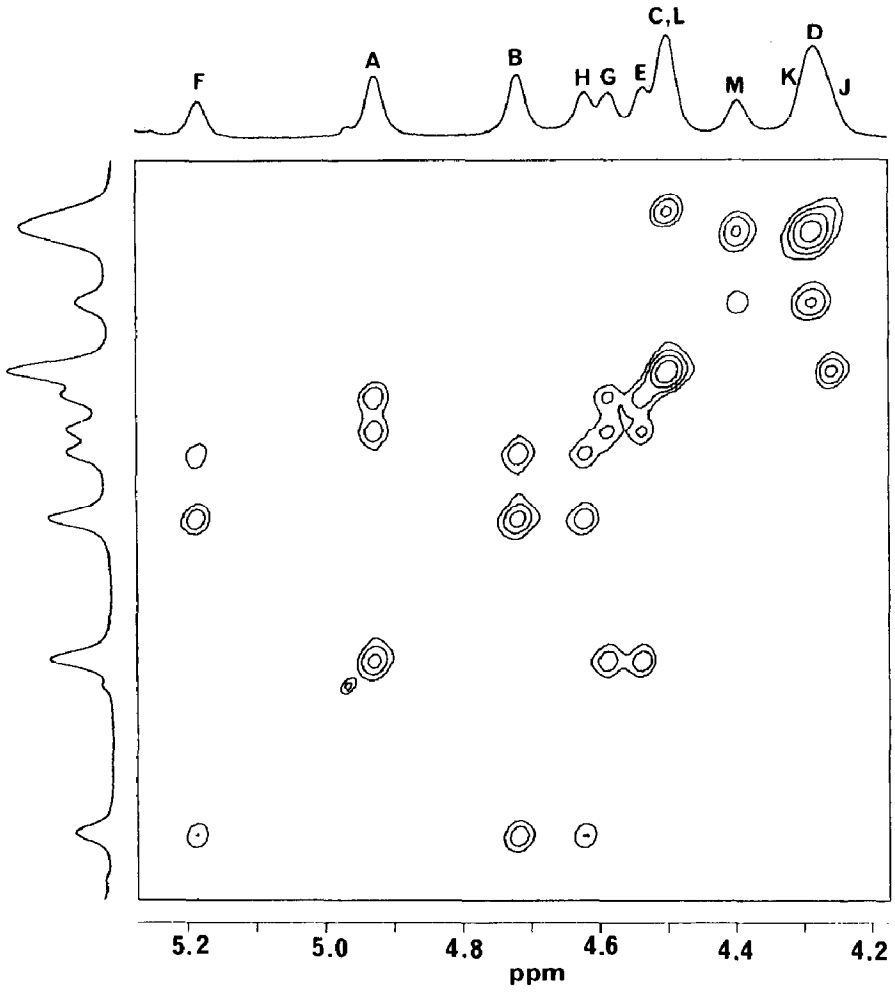

Fig. 3. The ^{1}H 2D-EXSY NMR spectrum of [ReCl(CO)$_3$(BMSF)] at −60 °C showing the four sets of exchanging methine protons. The labelling refers to Fig. 2.

rates of single site inversion [7,8]. Excellent fits between experimental and theoretical spectra were achieved for the five complexes studied, the high quality of fits confirming the correctness of the identification of the four sets of exchanging signals by the 2D-EXSY analysis.

Activation parameters based on the Arrhenius and Eyring rate theories were calculated in the usual way and the values are collected in Table 5. Certain consistencies in these values may be noted. Magnitudes of the $\Delta G^{\ddagger}$ parameter, calculated for 298.15 K, fall within the narrow ranges of 42.5–43.8 kJ mol^{-1} when sulphur inversion leads to *meso*-1 → DL-1 exchange, and 46.0–46.4 kJ mol^{-1} for DL-1 → DL-1 exchange. For selenium inversion corresponding values are about 20 kJ mol^{-1} larger and fall in the ranges 63.3–63.7 kJ mol^{-1} (*meso*-1 → DL-1) and 66.1–66.5 kJ mol^{-1} (DL-1 → DL-1). These narrow ranges clearly indicate negligible influence of halogen type on the inversion energies. The most significant feature of these values is that they are about 23 kJ mol^{-1} lower in magnitude than those for tricarbonylrhenium halide complexes with aliphatic thio- and seleno-ether ligands,

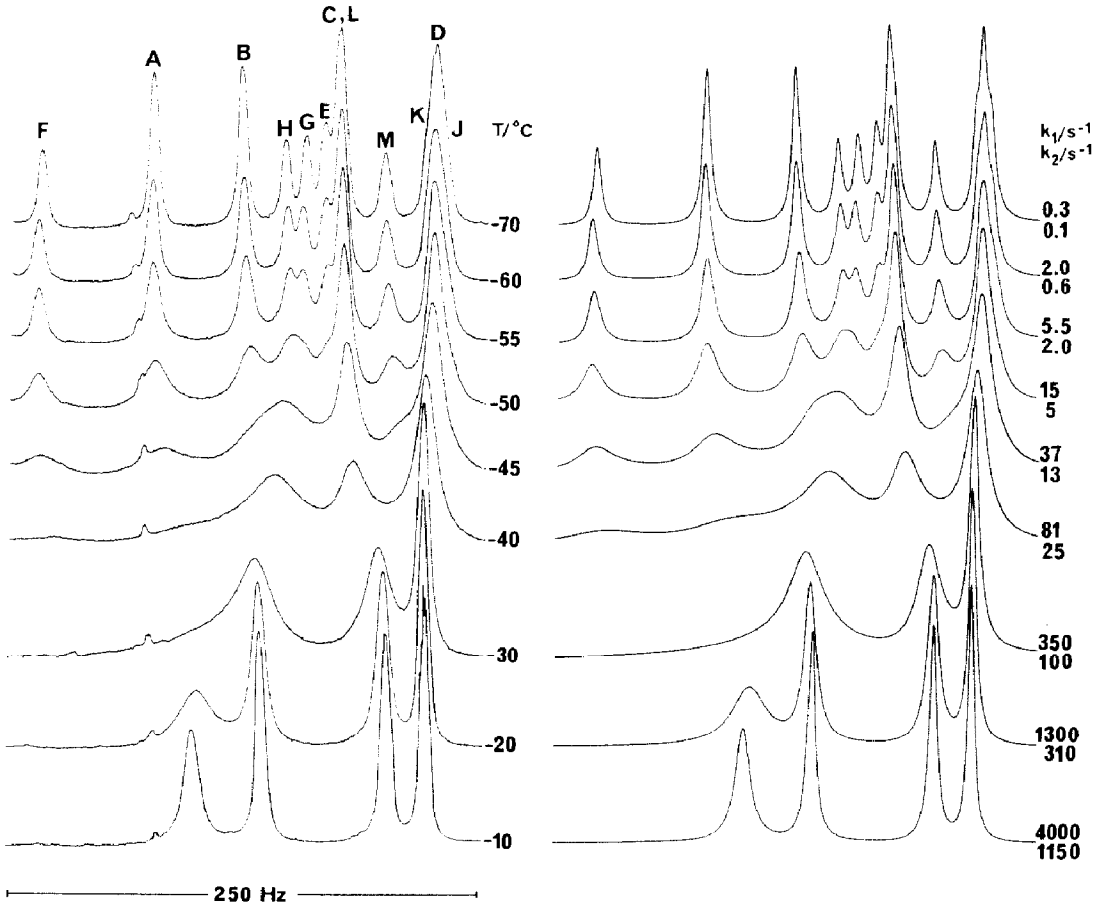

Fig. 4. Experimental (left) and computer simulated (right) ^{1}H NMR spectra of [ReCl(CO)$_3$(BMSF)] in the temperature range −70 to −10 °C. Best-fit rate constants k_1 and k_2 refer to *meso*-1 → DL-1 and DL-1 → DL-1 exchanges, respectively.

Table 5

Arrhenius and Eyring activation parameters for pyramidal chalcogen inversion (*meso* → DL) and (DL → DL) in the complexes **1**, **2**, **4**, **5** and **6**

	Complex	E_a (kJ mol^{-1})	$\log_{10}(A/s^{-1})$	$\Delta H^{\ddagger}$ (kJ mol^{-1})	$\Delta S^{\ddagger}$ (J K^{-1} mol^{-1})	$\Delta G^{\ddagger}$ (298 K) (kJ mol^{-1})
1	(*meso* → DL)	71.2 ± 1.0	17.8 ± 0.2	69.3 ± 1.0	90.0 ± 4.5	42.5 ± 0.3
	(DL → DL)	69.3 ± 1.5	16.9 ± 0.3	67.3 ± 1.5	71.6 ± 6.6	46.0 ± 0.5
2	(*meso* → DL)	69.2 ± 2.2	17.2 ± 0.5	67.3 ± 2.2	79.0 ± 9.6	43.8 ± 0.7
	(DL → DL)	69.0 ± 2.3	16.7 ± 0.5	67.1 ± 2.3	69.5 ± 10.3	46.4 ± 0.8
4	(*meso* → DL)	74.3 ± 1.3	14.7 ± 0.2	71.8 ± 1.3	27.1 ± 4.2	63.7 ± 0.03
	(DL → DL)	74.4 ± 1.3	14.2 ± 0.2	71.9 ± 1.3	18.0 ± 4.2	66.5 ± 0.03
5	(*meso* → DL)	74.1 ± 1.4	14.7 ± 0.2	71.6 ± 1.4	28.1 ± 4.6	63.3 ± 0.01
	(DL → DL)	74.1 ± 1.3	14.2 ± 0.2	71.6 ± 1.3	18.7 ± 4.2	66.1 ± 0.01
6	(*meso* → DL)	70.1 ± 1.4	14.0 ± 0.2	67.6 ± 1.4	14.4 ± 4.7	63.3 ± 0.02
	(DL → DL)	74.8 ± 2.1	14.3 ± 0.4	72.3 ± 2.2	19.9 ± 7.1	66.4 ± 0.04

namely $[ReX(CO)_3\{MeE(CH_2)_2EMe\}]$ (E = S, Se; X = Cl, Br, I) [17]. For example, the following two comparisons of $\Delta G^{\ddagger}$ values for *meso*-1 → DL interconversions are pertinent, $[ReBr(CO)_3\{MeS(CH_2)_2SMe\}]$ (63.2 kJ mol^{-1}, [17]) versus $[ReBr(CO)_3(BMSF)]$ (43.8 kJ mol^{-1}), and $[ReBr(CO)_3\{MeSe(CH_2)_2SeMe\}]$ (86.7 kJ mol^{-1} [17]) versus $[ReBr(CO)_3(BMSEF)]$ (63.3 kJ mol^{-1}).

These appreciably lower activation energies reflect the smaller ring strain effects of the pseudo-six-membered ferrocenophane rings compared to the five-membered chelate rings. Such ring size effects have been noted previously when comparing inversion energies of five- and six-membered chelate complexes, viz. $[PtXMe_3\{MeE(CH_2)_2EMe\}]$ and $[PtXMe_3\{MeE(CH_2)_3EMe\}]$ [18]. In such cases, however, the decreases in energy on going from five to six-membered rings was only 6–8 kJ mol^{-1}. The exceptionally low inversion energies in the present ferrocenophane complexes implies particularly easy access of the inverting chalcogens to the planar transition state configuration, and is likely to be associated with the high degree of flexibility of the E–Re–E portion of the ferrocenophane ring. This influence of ring flexibility is also evident in the earlier parts of this work involving $M(CO)_4$ and $PtXMe_3$ as metal moieties [2,3]. Comparison of inversion energies between $[W(CO)_4\{MeS(CH_2)_2SMe\}]$ [19] and $[W(CO)_4(BMSF)]$ [2] showed a lowering of 22.2 kJ mol^{-1}, and between $[PtBrMe_3\{MeS(CH_2)_nSMe\}]$ [18] and $[PtBrMe_3(BMSF)]$ falls of 19.8 ($n = 2$) and 12.8 ($n = 3$) kJ mol^{-1}. Clearly, the nature of the metal moiety plays a relatively minor role in influencing the chalcogen

Table 6

Fractional atomic coordinates [a] ($\times 10^4$) for $[ReCl(CO)_3(BMSF)]$

	x	*y*	*z*
Re	1404.8(2)	2638.4(1)	851.7(2)
Fe	−3241.2(10)	2220.9(5)	−2561.9(10)
S(1)	−1229(2)	1941(1)	1778(2)
S(2)	10(2)	3948(1)	−1010(2)
Cl	1813(2)	3579(1)	3385(2)
O(1)	986(7)	1386(4)	−2150(7)
O(2)	4630(6)	3830(4)	−51(9)
O(3)	3000(7)	1079(4)	3466(7)
C(1)	1091(7)	1885(4)	−1031(8)
C(2)	3422(8)	3390(5)	284(9)
C(3)	2414(8)	1664(4)	2503(8)
C(4)	−1179(9)	843(5)	3528(9)
C(5)	1337(9)	4893(5)	−2347(9)
C(6)	−2783(7)	1449(4)	37(7)
C(7)	−4302(6)	1637(4)	−333(7)
C(8)	−5249(8)	1189(4)	−1893(8)
C(9)	−4288(8)	722(4)	−2469(8)
C(10)	−2764(8)	878(4)	−1286(8)
C(11)	−1550(6)	3518(3)	−2793(7)
C(12)	−3078(7)	3731(4)	−3113(8)
C(13)	−4088(8)	3287(4)	−4681(9)
C(14)	−3113(8)	2818(4)	−5290(7)
C(15)	−1596(7)	2969(4)	−4161(7)

[a] Esd's, given in parentheses, are applicable to the least significant digits.

inversion rates, which are primarily a function of the magnitude of angle constraint for access to the planar transition state.

In the previous study of the platinum(IV) complexes $[PtXMe_3L]$ (L = BMSF, BMSEF) [3], high temperature fluxionality involving ligand rotation and scrambling

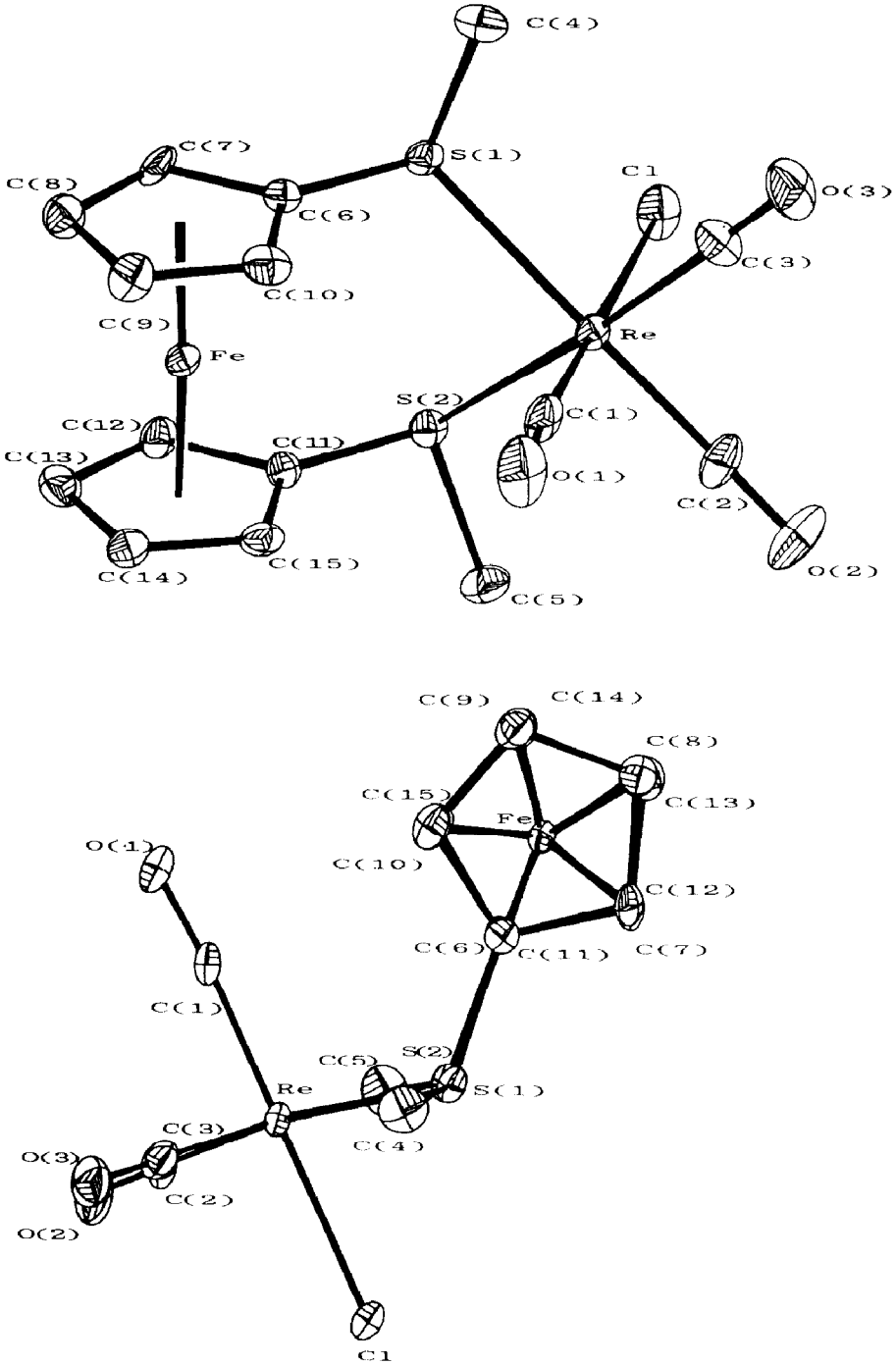

Fig. 5. Two views of the X-ray crystal structure of $[ReCl(CO)_3\{(C_5H_4SCH_3)_2Fe\}]$. Full data given in Tables 6–9.

Table 7

Bond distances (Å) [a] for [ReCl(CO)$_3$(BMSF)]

S(1)–Re	2.504(4)	S(2)–Re	2.512(4)
Cl–Re	2.478(3)	C(1)–Re	1.892(8)
C(2)–Re	1.920(8)	C(3)–Re	1.917(8)
C(6)–Fe	2.022(7)	C(7)–Fe	2.036(7)
C(8)–Fe	2.064(8)	C(9)–Fe	2.059(8)
C(10)–Fe	2.048(7)	C(11)–Fe	2.026(7)
C(12)–Fe	2.062(7)	C(13)–Fe	2.095(8)
C(14)–Fe	2.058(7)	C(15)–Fe	2.046(8)
C(4)–S(1)	1.802(8)	C(6)–S(1)	1.761(7)
C(5)–S(2)	1.818(8)	C(11)–S(2)	1.757(7)
C(1)–O(1)	1.195(8)	C(2)–O(2)	1.146(9)
C(3)–O(3)	1.134(8)	C(7)–C(6)	1.420(9)
C(10)–C(6)	1.434(9)	C(8)–C(7)	1.429(9)
C(9)–C(8)	1.432(10)	C(10)–C(9)	1.424(10)
C(12)–C(11)	1.447(8)	C(15)–C(11)	1.420(9)
C(13)–C(12)	1.447(10)	C(14)–C(13)	1.459(10)
C(15)–C(14)	1.403(9)		

[a] Esd's, given in parentheses, are applicable to the least significant digits.

of Pt-methyl environments was detected. It is thought highly likely that analogous fluxional processes are occurring in the present isoelectronic ReX(CO)$_3$ complexes, but unfortunately firm NMR evidence for this is lacking. The ^{13}C carbonyl signals were difficult to detect due to a combination of circumstances, namely (i) relatively small amounts of complex available, (ii) long spin-lattice relaxation times of the carbonyl carbons, and (iii) line broadenings of the carbonyl signals from the quadrupolar ^{185}Re and ^{187}Re nuclei. The use of ^{13}CO enriched complexes would seem essential for obtaining any definitive evidence for the likely carbonyl scrambling in these ReX(CO)$_3$ ferrocenophane complexes.

Table 8

Selected bond angles (°) [a] for [ReCl(CO)$_3$(BMSF)]

S(1)–Re–S(2)	80.0(2)		
C(1)–Re–S(1)	99.0(3)	Cl–Re–S(1)	80.3(2)
C(3)–Re–S(1)	96.4(3)	C(2)–Re–S(1)	169.5(2)
C(1)–Re–S(2)	98.6(3)	Cl–Re–S(2)	82.8(2)
C(3)–Re–S(2)	173.8(2)	C(2)–Re–S(2)	93.8(3)
C(6)–S(1)–Re	114.9(3)	C(11)–S(2)–Re	113.4(3)
C(6)–S(1)–C(4)	100.8(4)	C(11)–S(2)–C(5)	101.0(4)
C(7)–C(6)–S(1)	122.4(5)	C(12)–C(11)–S(2)	121.8(5)
C(10)–C(6)–S(1)	129.0(6)	C(15)–C(11)–S(2)	130.1(4)
C(10)–C(6)–C(7)	108.5(6)	C(15)–C(11)–C(12)	108.1(6)
C(8)–C(7)–C(6)	108.3(6)	C(13)–C(12)–C(11)	108.4(6)
C(9)–C(8)–C(7)	107.1(6)	C(14)–C(13)–C(12)	105.3(6)
C(10)–C(9)–C(8)	109.0(6)	C(15)–C(14)–C(13)	109.9(6)
C(9)–C(10)–C(6)	107.0(6)	C(14)–C(15)–C(11)	108.3(6)

[a] Esd's given in parentheses, are applicable to the least significant digits.

Table 9

Equations of selected least-squares mean planes

Cyclopentadienyl ring C(6)–C(10)				
$0.23474x + 0.75143y - 0.61664z = 0.73577$				
Deviations (Å)	C(6)	0.0009	C(9)	−0.0003
	C(7)	−0.0013	C(10)	−0.0006
	C(8)	0.0011	S(1)	0.0962
Cyclopentadienyl ring C(11)–C(15)				
$0.22688x + 0.75623y - 0.61371z = 4.07118$				
Deviations (Å)	C(11)	−0.0059	C(14)	−0.0030
	C(12)	0.0057	C(15)	0.0065
	C(13)	−0.0025	S(2)	0.0186

X-ray crystallography

Atomic parameters for the crystal structure of $[ReCl(CO)_3(BMSF)]$ are given in Table 6. Two views of the molecule drawn with the program ORTEP [20] and indicating the numbering scheme adopted are shown in Fig. 5. This displays the expected *fac*-octahedral coordination for Re, the chelating nature of the ligand and the *meso* relationship of the S-CH_3 groups. Bond distances and selected bond angles are noted in Tables 7 and 8 respectively.

The iron–carbon distances range from 2.022(7) to 2.095(8) Å, which compare favourably with other ferrocene derivatives. The carbon–carbon distances in the cyclopentadienyl rings vary from 1.403(9) to 1.459(10) Å, and the C–C–C bond angles within the two rings vary from 105.3(6)° to 109.9(6)°. The Re–S bond lengths are 2.504(4) and 2.512(4) Å, values which are comparable with the values found in compounds containing Re^I bonded to S [21–23].

Inspection of the bond angles at Re (Table 8) shows that there is considerable distortion from a regular octahedral structure at Re, with an S–Re–S angle of 80.0(2)°. Differences in the ferrocenyl exocyclic C–C–S bond angles (means 122.1 and 129.5°) are also observed. These can be compared with values of 122.8 and 129.2° in 1,3-dithia-2-phenylarsino[3]ferrocenophane [24] and 123.4 and 128.2° in 1,3-dithia-2-selena[3]ferrocenophane [25]. This is a structural feature which is common to ferrocenophanes of this type.

Equations for least-squares mean planes of the cyclopentadienyl rings are given in Table 9. The rings are planar within limits of error and adopt an eclipsed configuration (Fig. 5). The cyclopentadienyl rings can be considered to be parallel, the dihedral angle between them being only 0.6°. This result is similar to that found in $[Fe(C_5H_4S)_2]AsC_6H_5$, [24] but compares with dihedral angles of 2.9 and 2.4° for the compounds $[Fe(C_5H_4S)_2]Y$ (Y = S [26] or Se [25]) and 1.9° for $[Fe(C_5H_4SPr^i)_2]PdCl_2$ [27]. The two S atoms are unsymmetrically displaced from the respective ring planes by 0.1 and 0.02 Å, giving rise to a non-bonded S–S separation of 3.224 Å.

Acknowledgements

We wish to thank the University of Exeter for a Frank Southerden Scholarship (to N.J.L.), and the S.E.R.C for use of the high-field NMR service (University of Warwick).

References

1 E.W. Abel, S.K. Bhargava and K.G. Orrell, Prog. Inorg. Chem., 32 (1984) 1.
2 E.W. Abel, N.J. Long, K.G. Orrell, A.G. Osborne, V. Šik, P.A. Bates and M.B. Hursthouse, J. Organomet. Chem., 367 (1989) 275.
3 E.W. Abel, N.J. Long, K.G. Orrell, A.G. Osborne and V. Šik, J. Organomet. Chem., 378 (1989) 473.
4 D.F. Schriver, Manipulation of Air-Sensitive Compounds, McGraw-Hill, New York, 1969.
5 W. Hieber, R. Schuh and H. Fuchs, Z. Anorg. Allg. Chem., 248 (1941) 243.
6 M.M. Bhatti, Ph.D. Thesis, University of Exeter, 1980.
7 E.W. Abel, T.P.J. Coston, K.G. Orrell, V. Šik and D. Stephenson, J. Magn. Reson., 70 (1986) 34.
8 E.W. Abel, I. Moss, K.G. Orrell, V. Šik and D. Stephenson, J. Chem. Soc., Dalton Trans., (1987) 2695.
9 D.A. Kleier and G. Binsch, J. Magn. Reson., 3 (1970) 146.
10 D.A. Kleier and G. Binsch, DNMR3 Program 165, Quantum Chemistry Program Exchange, Indiana University, 1970.
11 M.B. Hursthouse, R.A. Jones, K.M.A. Malik and G. Wilkinson, J. Am. Chem. Soc., 101 (1979) 4128.
12 A.C.T. North, D.C. Phillips and F.S. Matthews, Acta Crystallogr., A, 24 (1968) 351.
13 G.M. Sheldrick, SHELX-84, Program for Crystal Structure Solution, private communication.
14 G.M. Sheldrick, SHELX-76, Program for Crystal Structure Determination and Refinement, University of Cambridge, 1976.
15 D.T. Cromer and J.B. Mann, Acta Crystallogr., A, 24 (1968) 321.
16 D.T. Cromer and D. Liberman, J. Chem. Phys., 53 (1970) 1891.
17 E.W. Abel, S.K. Bhargava, M.M. Bhatti, K. Kite, M.A. Mazid, K.G. Orrell, V. Šik, B.L. Williams, M.B. Hursthouse and K.M.A. Malik, J. Chem. Soc., Dalton Trans., (1982) 2065.
18 E.W. Abel, A.R. Khan, K. Kite, K.G. Orrell and V. Šik, J. Chem. Soc., Dalton Trans., (1980) 1175.
19 E.W. Abel, I. Moss, K.G. Orrell and V. Šik, J. Organomet. Chem., 326 (1987) 187.
20 C.K. Johnson, ORTEP II: A Fortran Thermal Ellipsoid Plotting Program Crystal Structure Illustrations, ORNL Report 3794, Oak Ridge National Laboratory, Oak Ridge, Tennessee, U.S.A., 1971.
21 R. Mattes and H. Weber, J. Organomet. Chem., 178 (1979) 191.
22 G. Thiele, G. Liehr and E. Lindner, J. Organomet. Chem., 70 (1974) 427.
23 W. Harrison, W.C. Marsh and J. Trotter, J. Chem. Soc., Dalton Trans., (1972) 1079.
24 A.G. Osborne, R.E. Hollands, R.F. Bryan and S. Lockhart, J. Organomet. Chem., 288 (1985) 207.
25 A.G. Osborne, R.E. Hollands, J.A.K. Howard and R.F. Bryan, J. Organomet. Chem., 205 (1981) 395.
26 B.R. Davis and I. Bernal, J. Cryst. Mol. Struct., 2 (1972) 107.
27 B. McCulloch, D.L. Ward, J.D. Woolins and C.H. Brubaker, Jr., Organometallics, 4 (1985) 1425.